The 1st International Symposium on Multi-Robot and Multi-Agent Systems (MRS 2017)
December 4-5, 2017, Los Angeles, CA, USA

Tracking Wildlife with Multiple UAVs: System Design, Safety and Field Experiments

Haluk Bayram, Nikolaos Stefas, Kazim Selim Engin, Volkan Isler

Abstract— **We present a multi-UAV system capable of localizing radio tagged animals. Each UAV carries a Yagi antenna and is capable of obtaining bearing-measurements by using the directionality of the signal emitted from the tag. In this paper, we address the following question: given a set of measurement locations, should the UAVs move in coordination and obtain synchronized measurements, or should they move independently? For each scenario, we present a path planning algorithm. The algorithms are compared in simulations. We also present a complete system implementation with three UAVs and results from field experiments.**

I. Introduction

Wildlife monitoring is important for biologists who study animals and their habitats. The most commonly used technique for tracking animals is Very High Frequency (VHF) radio-tracking, also known as wildlife telemetry [1]. This technique involves attaching a radio transmitter to the animal of interest and a radio receiver tuned at a specific frequency frequency. For large animals such as bears and wolves, the radio transmitter is put on a collar. These collars are developed to work for long periods of time. However, their transmission range is only a couple of kilometers. Tracking wildlife is challenging because the researchers must first establish contact with the signal in remote and potentially dangerous animal habitats. Once the signal is detected, the directionality of the signal is utilized to obtain bearing measurements. The animal is localized either by converging to the source of the signal by following its gradient or by triangulating multiple bearing measurements.

To mitigate some of these challenges, researchers have started using Uninhabited Aerial Vehicles (UAV) for animal tracking [2]–[5]. In particular, multi-rotor UAVs can rotate in-place to take bearing measurements, they are easy to deploy and relatively inexpensive. Therefore, they have the potential to be an ideal system for automated animal localization in hard to access or dangerous areas [6].

However, despite their advantages multi-rotor UAVs have limited battery capacity which is especially critical considering that they have to spend significant amount of time taking measurements. If the targets are highly mobile, taking multiple measurements become difficult. We present an energy-aware multi-UAV system which can overcome these challenges and can localize targets faster and more accurately over large areas as illustrated in Figure 1.

The authors are with the Department of Computer Science & Engineering, University of Minnesota, Minneapolis, USA. {hbayram, stefa125, engin003, isler}@umn.edu. This work is supported in part by a Minnesota State LCCMR grant and NSF grants #1111638, #1525045 and #1617718.

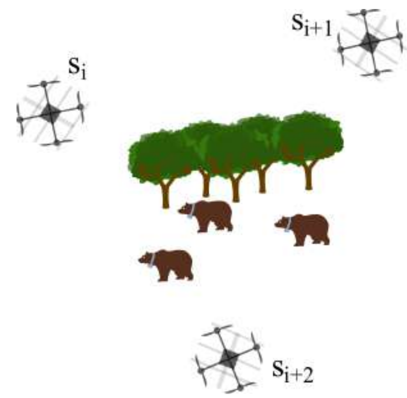

Fig. 1. The Multi-UAV Wildlife Tracking Problem: collared animals are to be localized. The goal is to make use of multiple UAVs in order to localize the targets in such a way that the localization uncertainty is below a desired level. In this illustration, the 3-UAV team is taking bearing measurements (coordinated by the team leader) from their measurement locations s_i, s_{i+1}, s_{i+2} to localize the collared animals.

It is also possible to use signal strength or time of arrival to obtain range-related information [7], [8]. Even though signal strength or time of arrival is a function of distance, the exact characteristics of the function can be highly environment dependent and it is difficult to extract direct range information [5]. In this paper, we focus on bearing because it is much more reliable and does not require environment specific calibration.

The problem of localizing targets by actively choosing measurement locations has been previously addressed in the literature: In [9], a Lyapunov based approach is proposed to track a stationary or moving target in a coordinated manner. In this work, the proposed approach is evaluated through simulations. The work in [10] proposes algorithms with proven performance bounds for actively locating a static target using multiple autonomous surface vehicles equipped with bearing sensors. In [11], multiple UAVs carrying a camera are tracking mobile targets using a team of aerial robots in an indoor setting. The authors present an algorithm to assign trajectories for each UAV in order to maximize the tracking quality. In our work, we first present a novel approach for taking measurements where the UAVs rotate in place to obtain bearing measurements. We adapt our previous work [12] to compute measurement locations and address the following questions: Should the UAVs move independently to minimize the total (or maximum) tour length, or should they act together? Coupling the motion of the UAVs can result in longer trajectories however it can also lead to better bearing measurements, hence better localization performance. We present two strategies (one for each scenario) which are compared in simulations. The proposed approach is also implemented on multiple quadrotors and its effectiveness is evaluated through a series of simulations and field experiments.

Problem Statement: The objective is to compute measurement locations for multiple UAVs so as to localize animals up to a desired localization uncertainty. Formally, given an environment $\mathcal{T} \subset \mathbb{R}^2$, compute the measurement locations $S = \{s_1, ..., s_n\}$ and the tour τ visiting them for each UAV such that the following criteria are satisfied:

- the time spent in visiting these locations and taking measurements is minimized,
- the resulting localization uncertainty U for each location in $\mathcal{T}$ is below the desired uncertainty $U^{\star}$,
- collision avoidance among UAVs is guaranteed.

The contributions of the paper can be summarized as follows: We present (i) a planning algorithm using coordinated and non-coordinated data gathering strategies to localize radio-tagged animals using bearing measurements, (ii) a comparison of these strategies to show the localization performance when the target is moving, (iii) the design of a multi-UAV system with a directional antenna, and onboard computation and wireless communication capabilities, and (iv) the implementation of the coordinated data gathering approach on the multi-UAV system.

II. Data Gathering with $3k$ Aerial Robots

In this section, we present the coordinated data gathering strategy for multiple UAVs. For simplicity, we assume that the number of robots is a multiple of three. At a high level, the $3k$ robots proceed as follows.

- Determine measurement locations.
  - Cover the candidate target areas with measurement disks with radius R such that the localization uncertainty is guaranteed up to a certain level within these disks.
  - Compute measurement locations based on these disks
- Compute trajectories
  - Compute a tour for all the centers of the disks
  - Split the tour into k sub-tours (one for each aerial robot team) considering battery constraint
  - Compute a trajectory for each robot using their corresponding sub-tour
- Execute the mission in a coordinated manner
  - Follow the assigned trajectories
  - Take bearing measurements (each team starts to take bearing measurements at the same time)
- Estimate the target location
  - Merge the bearing measurements
  - Localize the targets using the gathered measurements based on the localization uncertainty model

We now elaborate on these steps. First, we introduce the uncertainty model which measures the localization uncertainty for given two bearing measurements. Next, we present how to determine the measurement locations and tours. Following, we propose the coordinated measurement-taking approach. Last, we briefly explain how to estimate the target location using beating measurements.

A. Localization Uncertainty Model

To estimate a target's location from two bearing measurements, triangulation is the most commonly used approach. In the absence of measurement noise, the target's true location would be found by intersecting two bearing measurements. However, a real sensor produces bearing measurements corrupted with a noise, which is generally modeled by Gaussian distribution with known mean and variance. Because of the presence of noise, the intersection of two bearing measurements does not yield true target location, but estimate target location with some uncertainty. The geometric dilution of precision (GDOP) is widely used to measure the uncertainty of the estimate [13]. Formally, given two measurements from locations s_1 and s_2 for a target at location w in a 2D environment and measurement noise with variance σ^2, the localization uncertainty U is given by [12]

$$U(s_1, s_2, w) = \frac{d(s_1, w)d(s_2, w)}{|sin\measuredangle s_1 w s_2|}\pi\sigma^2 \tag{1}$$

where $d(s_i, w)$ is the distance between the measurement location s_i and target location w.

B. Measurement Locations & Tours

In determining the measurement locations for a given target candidate area, we make use of the sensor placement scheme in [14]. In this scheme, for a desired uncertainty level $U^{\star}$ and bearing measurement noise variance σ^2, when three measurements are taken from the vertices of an equilateral triangle whose circumcircle is a disk with radius $R' = R\sqrt[3]{4}$, the localization uncertainty within the disk D (co-centric with the circumcircle) with radius $R = 2\sqrt{U^{\star}/(\pi\sigma^2)}$ is guaranteed to be less than $5.5U^{\star}$.

By covering candidate target areas with disks $\mathcal{D}$, each disk $D \in \mathcal{D}$ contains 3 measurement locations. Given the rectangular candidate target area $\mathcal{T}$, the desired localization uncertainty $U^{\star}$ and the bearing measurement noise variance σ^2, Algorithm 1 computes the measurement disks $\mathcal{D}$ and the measurement locations $\mathcal{S}$ located at the vertices of the equilateral triangles within these disks. A sample scenario can be seen in Figure 2. Once the measurement disks $\mathcal{D}$ are obtained, a TSP tour τ is generated using Concorde TSP Solver [15] for the centers of the disks. Then, the tour τ is split into sub-tours considering either the number of teams or the energy budget. The general strategy of splitting a TSP tour into roughly equal size sub-tours is presented in [16] (Algorithm `k-SPLITOUR`). When the splitting is done based on the number of teams and the teams have sufficient energy to complete each sub-tour, the sub-tours are computed based on the number of teams. Otherwise, since the energy is not

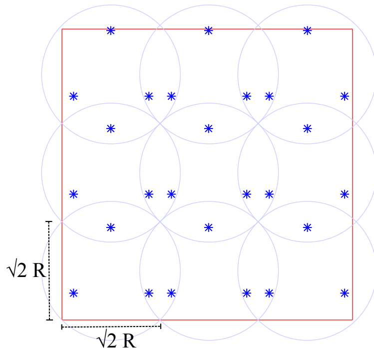

Fig. 2. Measurement disks with radius R and corresponding measurement locations (denoted by stars) for a given rectangular area $\mathcal{T}$, desired localization uncertainty $U^\star$ and bearing measurement noise σ. The disks and measurement locations are computed by `Compute-Measurement-Locations` (Algorithm 1).

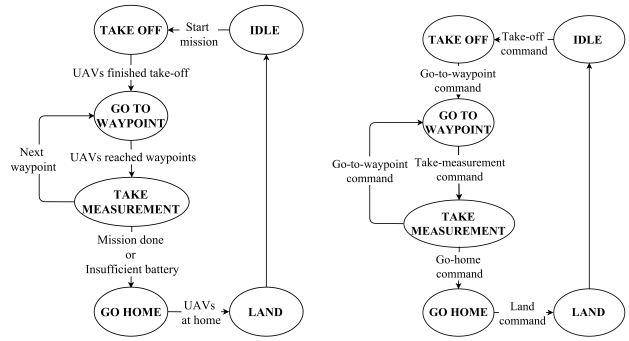

(a) Task Coordinator (b) Task Handler

Fig. 3. (a) Finite state machine which the leader executes for coordinating its team. At each state, the leader broadcasts corresponding commands to its members and waits for responses from the members that the command has been executed. (b) Finite state machine which the task handler executes for the localization task. State transitions occur when the corresponding command is received.

sufficient for any of sub-tours, the splitting is done based on the energy budget.

Algorithm 1 `Compute-Measurement-Locations`

Input: $\mathcal{T}$, $U^\star$ and σ^2
$R \leftarrow 2\sqrt{U^\star/(\pi\sigma^2)}$ {Measurement disk radius}
$R' \leftarrow R/\sqrt[3]{4}$ {Radius of circumcircle of the equilateral triangle}
$\mathcal{S} \leftarrow \emptyset$ {Initialize the measurement locations}
$\mathcal{D} \leftarrow \emptyset$ {Initialize the measurement disks}
$\Delta d \leftarrow R\sqrt{2}$ {Displacement of disks}
$[x_0, y_0] \leftarrow$ left bottom coordinate of the area $\mathcal{T}$
for $i = 1$ to width($\mathcal{T}$)/Δd **do**
  for $j = 1$ to height($\mathcal{T}$)/Δd **do**
    $[x_d, y_d] \leftarrow [x_0 + (2i-1)\Delta d/2, y_0 + (2j-1)\Delta d/2]$
    $\mathcal{D} \leftarrow \mathcal{D} \cup D([x_d, y_d], R)$ {New measurement disk}
    $s_1 \leftarrow [x_d - R'\sqrt{3}/2, y_d - R'/2]$ {1st measurement location}
    $s_2 \leftarrow [x_d + R'\sqrt{3}/2, y_d - R'/2]$ {2nd measurement location}
    $s_3 \leftarrow [x_d, y_d + R']$ {3rd measurement location}
    $\mathcal{S} \leftarrow \mathcal{S} \cup \{s_1, s_2, s_3\}$
  end for
end for
Output: $\mathcal{D}$ and $\mathcal{S}$

C. Coordinated Data Gathering

If the targets to be localized are stationary, the measurements do not have to be synchronized. Therefore, the time at which the measurement are taken do not have any effect on the estimation of the target location. If the targets are moving, three measurements taken at different times for a measurement disk may become inconsistent. To minimize this effect, we assign 3 robots to each tour. The robots synchronize their measurements. We choose one robot of the team as the leader, which is responsible for coordinating the whole team. The leader and members execute a finite state machine with six states (`IDLE`, `TAKE-OFF`, `GO-TO-WAYPOINT`, `TAKE-MEASUREMENT`, `GO-HOME`, `LAND`) as shown in Figure 3. At each state, the leader sends the relevant command to the team and goes into the waiting-mode. Once the members execute the command, they send back the message that they have completed the command. When the leader receives command-completion messages from all the members, the state transition occurs, and then the leader sends the next command to the team. The collision avoidance is accomplished by assigning different altitudes to each robot. During the mission, they fly at their predefined altitudes.

At the beginning of the mission, all the robots are in `IDLE` state. When the leader receives the start-mission command from the ground station, it sends the take-off command to the team and the team goes into `TAKE-OFF` state. After all the robots take off and send the take-off completion message to the leader, the leader send the go-to-waypoint command to the team and the team goes into `GO-TO-WAYPOINT` state. After reaching the waypoint, the robots send the command completion message to the leader. Once the leader receives all the completion messages from the team, it sends the take-measurement command to the team and the team goes into `TAKE-MEASUREMENT` state. Therefore all the members in a team start taking bearing measurements at the same time. `GO-TO-WAYPOINT` and `TAKE-MEASUREMENT` states are repeated until the mission is done or the leader receives an insufficient battery message. In case of insufficient battery, the leader sends the go-home command to the team and then coordinates the landing.

D. Estimating Target Location

After completing the mission, from each disk D, we have three bearing measurements taken from locations s_1, s_2 and s_3 at the vertices of the equilateral triangle inside the disk D. For each triplet of bearing measurements, we choose the best pair, which is the pair with the lowest localization uncertainty, in order to estimate the target location:

- Intersect each measurement pair i and j in order to get the estimate location $w_{i,j}$ of the target.

TABLE I
LOCALIZATION ERROR (MEAN & STANDARD DEVIATION) FOR COORDINATED & NON-COORDINATED APPROACHES

	Target speed		
	1 m/sec	2 m/sec	4 m/sec
Coordinated	15.0 - 22.8	16.4 - 24.1	17.6 - 26.8
Non-coordinated	16.9 - 23.5	24.7 - 29.8	36.5 - 37.8

- To evaluate these three estimates, the localization uncertainty $U_{i,j}$ for each estimate is computed using Equation 1.
- The smallest of the localization uncertainties $U_{i,j}$ is chosen to compute the final estimate location of the target.

III. SIMULATIONS

In this section, we investigate the benefits of coordination. For this purpose, we compare the coordinated approach with the non-coordinated one in which the tours are computed for all the robots by considering the energy constraint and there is no synchronization in taking measurements.

We run coordinated and non-coordinated approaches 1000 times for the varying target speed $v = 1$ m/sec, 2 m/sec, 4 m/sec. The target performs a random walk within the candidate target area. In the work [3] on Minnesotan bears' behavioral response to aerial vehicles, a maximum movement rate increases up to 2.3 m/sec when the UAV is near of the bear. Since one of the goals in this work is to localize bears in Minnesota, we choose the varying speed levels for the target as consistent with the bears' movement. The other parameters are chosen as follows: the bearing noise $\sigma = \pi/6$ radians, desired localization uncertainty $U^\star = \pi 10^2$ (corresponding to the area of a disk with radius 10 meters), and the candidate target area 360×205 m^2. The UAVs can fly at a speed of 5 m/sec for 10 minutes. Each measurement takes 2 minutes. For target localization, the estimation method in Section II-D is used.

The simulation results for the localization error (mean and standard deviation) are presented in Table I. For low target speed, the localization performance of the approaches are similar. When target speed increases, the non-coordinated approach deteriorates more than the coordinated one.

Figure 4 shows the results obtained when the target speed is 4 m/sec. Since the coordinated approach can locate the target up to a localization error of 10 meters in most of the trials, it can be said that the faster the target moves the more the coordinated approach outperforms the non-coordinated one. The increase in the target's speed does not affect the localization performance of the coordinated approach as much as the non-coordinated one, which means the coordinated approach is more robust to the change in the target's speed.

IV. SYSTEM DESCRIPTION

In this section, we describe the hardware and software infrastructure of the system.

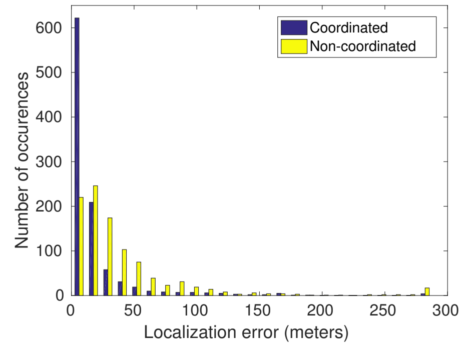

Fig. 4. Localization errors for coordinated and non-coordinated approaches when the target performs a random walk at the speed of 4 m/sec.

Fig. 5. Three aerial vehicles with a 3-element Yagi antenna mounted underneath.

A. Hardware Components

This work requires multiple aerial vehicles capable of autonomous navigation, onboard computation and wireless communication. The aerial robotic vehicles developed for this work are based on the quadrotor DJI Matrice 100 shown in Figure 5. A GPS and compass module provides autonomous GPS waypoint navigation with a horizontal and vertical hovering accuracy of 2.5 and 1 meters respectively. Maximum hovering time was measured at 12 minutes. Each system is equipped with the NVIDIA Jetson TX1 acting as the onboard processor and running an Ubuntu Linux operating system. The robots can communicate with each other over a wireless local network, which is established by a Wi-Fi router mounted on one of the robots. In case of any unexpected behavior that is observed from any of UAVs, the mission software can be overridden by the remote-controller.

Signal detection is enabled through a Yagi antenna located at the bottom of the UAV. An RTL-SDR USB signal receiver is deployed for analog-to-digital signal conversion for RTL2832 based DVB-T receivers with an IQ data format. The signal transmitter (animal's collar) is a Telonics MOD-500 VHF 163.900 MHz radio transmitter and operates in two modes: active and inactive. In active mode 80 pulses of 15 msec width are transmitted every minute. In inactive mode the transmitter conserves energy and the number of pulses drops to 40 per minute.

B. Software Modules

Since our aerial platforms provide ROS interface with the hardware components, we developed a ROS-based software with "Communication Node", "Task Handler Node" and "Task Coordinator Node" (Figure 6) to implement the proposed approach. The ground station is used to start the mission by sending a start-mission command to the leader.

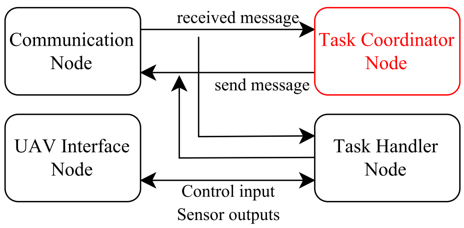

Fig. 6. ROS-based software architecture. The leader has an additional node named as "Task Coordinator" running the finite state machine in Figure 3(a). Each team member has the node "Task Handler" running the finite state machine in Figure 3(b).

The communication nodes differ based on whether the UAV is leader or not. While the leader UAV establishes two-way TCP socket with the member UAVs and the ground station, the member UAVs connect only to the leader. So, the resulting network topology becomes a star topology where the leader is in the center.

The leader has also an additional ROS node (Task Coordinator) which is responsible for coordinating the mission. This node runs the state machine depicted in Figure 3(a). Task Handler node executing the finite state machine in Figure 3(b) is common to all the UAVs.

To capture the received signal from the antenna, we use `rtl_sdr` software package [17], which is an IQ recorder for RTL2832 based DVB-T receivers.

V. Field Experiments

We have conducted four sets of field experiments at Cedar Creek Ecosystem Science Reserve where the wildlife biologists plan to tag wild animals with VHF collars: (1) coordinated navigation, (2) single stationary target localization, (3) multi-target localization, and (4) localization of a moving target. The collar was deployed at a known location within the candidate target area. The bearing noise standard deviation was set to $\sigma = \pi/6$ radians. The desired localization uncertainty $U^\star$ was set to 100π and 56π m^2 for the stationary target experiment, and multi-target and moving target experiments, respectively. These uncertainties correspond to the areas of disks with radius 10 meters and 7.5 meters. Given the candidate area, $U^\star$ and σ, the measurement locations and corresponding routes are generated as shown in Figure 7.

To see the effect of altitude variation on the measurements, we placed the collar 300 meters away from the UAV, then took bearing measurements for 10, 15 and 30 meter altitudes. The results reveal that the higher altitude provides more reliable bearing measurements. For the safety, the altitude difference between neighboring UAVs is chosen as 10 meters. Therefore, the altitudes for UAVs are set to 30, 40, 50 meters.

First, we tested the performance of the coordinated navigation in which the UAVs execute their mission without taking

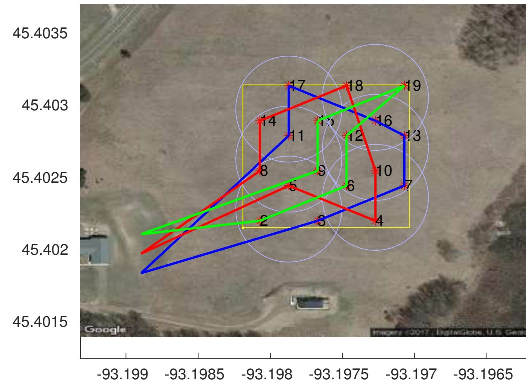

Fig. 7. Measurement locations and tours for each UAV. As described in Section II-B, given a rectangular candidate target area, six disks are generated to cover the area and three measurement locations are determined for each disk.

Fig. 8. Experiment for coordinated navigation. The UAVs navigate to the measurement locations in a coordinated manner (as described in Figure 3) without taking measurements. They can visit all the measurement locations with one battery since they do not take measurements.

measurements. In this experiment, the leader coordinates the whole mission. As shown in Figure 8, the UAVs completed the coordinated mission successfully.

Second, we run the full algorithm to localize one stationary target in an area of 160×105 m^2. After taking the third measurement, one of the UAVs sends the low battery message to the leader. Then, the leader broadcasts the go-home and land commands. After replacing the batteries, the team continues their mission from the next measurement location and completes the whole mission within 15 minutes. The resulting trajectories can be seen in Figure 10. The error on the target localization is about 29 meters.

Figure 9 shows the bearing measurements taken from the measurement locations. Using the estimation method described in Section II-D, the target location is estimated from these measurements.

Third, we conducted multi-target localization experiment. In this experiment, the three radio-tags with different transmitting frequencies are placed in the known locations. The UAVs take bearing measurements for each tag frequency from the vertices of the triangle. The localization results are shown in Figure 11. The bearing measurements are denoted by red line. Circles and crosses represent the true and estimate target locations, respectively. The UAVs estimate the tags with the localization error of 18.2 meters, 3.7 meters and

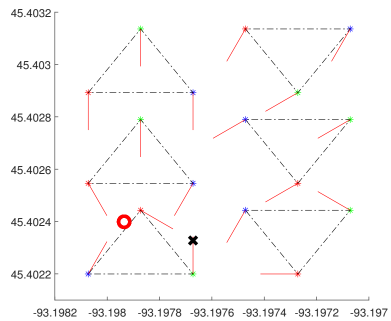

Fig. 9. Bearing measurements (red lines) taken for one stationary target from the measurements locations (stars). Circle and cross signs denote the true and estimate target locations, respectively.

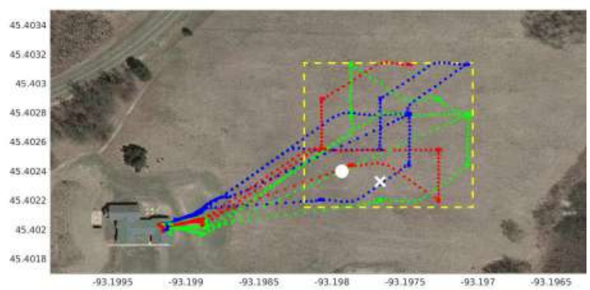

Fig. 10. The UAVs' trajectories in the experiment of localizing one stationary target.

10.7 meters.

In the last experiment, a person carrying the collar follows an arbitrary trajectory with an average speed of 0.56 m/sec in an area of 40×120 m^2. The GPS location of the person is recorded as ground truth. UAVs take measurements from three triangles which are given different colors in Figure 12. The target trajectory is colored according to the triangles the UAVs are at that particular time. The UAVs take one measurement from each of location and obtain an estimate. The estimates of the target location are plotted as crosses for each measurement set.

VI. Conclusion

In this paper, we presented a novel multi-UAV system that can localize VHF radio collared animals. At a high-level the data gathering strategy is to compute measurement locations along with tours to visit them. Each tour is assigned to a team of three robots. The teams operate independently. The three robots in each team execute a coordinated strategy in which the leader signals when to navigate to the next measurement location, take measurements, and when to go home in case of emergency. It was shown that the coordinated motion outperforms the non-coordinated motion in terms of the localization quality when the target is moving. We also validated the system in a series of field experiments using three autonomous aerial robots equipped with an on-board computer, directional antenna, and signal receiver.

In our future work, we plan to speed up the measurement process by eliminating the need to stop and rotate in place.

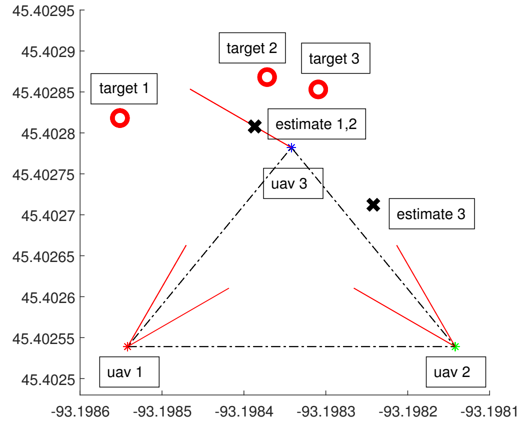

Fig. 11. Experiment for localizing multiple radio-tags. Each UAV takes one measurement for each of three radio-tags from their measurement location. Some of these bearing measurements coincide with one another. The bearing measurements are denoted by red line. Circles and crosses represent the true and estimate target locations, respectively. The estimate locations of the tags 1 and 2 coincide with each other. The radio-tags are located within the localization error of 18.2 meters, 3.7 meters and 10.7 meters.

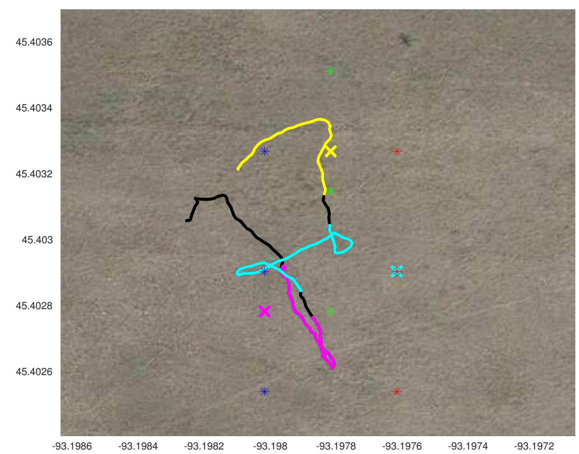

Fig. 12. Experiment for localizing a moving target. Measurement locations are denoted by stars and the estimate target locations are represented as crosses. The target is moving with an average speed of 0.56 m/sec in an area covered by three measurement triangles (nine measurement locations). The three measurements from each triangle generate an estimate location shown in a dedicated color (purple, cyan, yellow). The target's trajectory is colorized based on location (current triangle) of the UAVs. The target follows the black part of the trajectory when UAVs are moving.

We will also replace the Wi-Fi module with an XBee module in order to have more reliable and long range communication. From the theoretical point of view, we would like to obtain performance bounds on the cost and quality of the tours in terms of localization time. Our previous work in the domain [18], [19] for single robots will provide a starting point.

Acknowledgment

We thank Dr. Forest Isbel, Dr. Mark Ditmer and Cedar Creek Ecosystem Science Reserve staff for their help in experiments.

REFERENCES

[1] L. D. Mech and S. M. Barber, "A critique of wildlife radio-tracking and its use in national parks - a report to the U.S. National Park Service," Tech. Rep., 2002.

[2] R. J. Bamberger, J. G. Moore, R. P. Goonasekeram, and D. H. Scheidt, "Autonomous geo location of rf emitters using small, unmanned platforms," *Johns Hopkins APL Technical Digest*, vol. 32, no. 3, pp. 636–646, 2013.

[3] M. Ditmer, J. Vincent, L. Werden, J. Tanner, T. Laske, P. Iaizzo, D. Garshelis, and J. Fieberg, "Bears show a physiological but limited behavioral response to unmanned aerial vehicles," *Current Biology*, vol. 25, no. 17, pp. 2278–2283, 2015.

[4] K. VonEhr, S. Hilaski, B. E. Dunne, and J. Ward, "Software defined radio for direction-finding in uav wildlife tracking," in *IEEE Int. Conf. on Electro Information Technology*, 2016, pp. 464–469.

[5] H. Bayram, K. Doddapaneni, N. Stefas, and V. Isler, "Active localization of vhf collared animals with aerial robots," in *2016 IEEE Int. Conf. on Automation Science and Engineering*, 2016, pp. 934–939.

[6] A. Lucieer, D. Turner, D. H. King, and S. A. Robinson, "Using an Unmanned Aerial Vehicle (UAV) to capture micro-topography of Antarctic moss beds," *International Journal of Applied Earth Observation and Geoinformation*, vol. 27, Part A, pp. 53–62, 2014.

[7] B. Charrow, N. Michael, and V. Kumar, *Active Control Strategies for Discovering and Localizing Devices with Range-Only Sensors*. Springer International Publishing, 2015, pp. 55–71.

[8] Y. Lin, H. Kastein, T. Peterson, C. White, C. G. Lowe, and C. M. Clark, "A multi-AUV state estimator for determining the 3D position of tagged fish," in *IEEE/RSJ International Conference on Intelligent Robots and Systems*, 2014, pp. 3469–3475.

[9] R. Wise and R. Rysdyk, "Uav coordination for autonomous target tracking," in *AIAA Guidance, Navigation, and Control Conference and Exhibit*, 2006, p. 6453.

[10] J. Vander Hook, P. Tokekar, and V. Isler, "Algorithms for cooperative active localization of static targets with mobile bearing sensors under communication constraints," *IEEE Transactions on Robotics*, vol. 31, no. 4, pp. 864–876, Aug 2015.

[11] P. Tokekar, V. Isler, and A. Franchi, "Multi-target visual tracking with aerial robots," in *IEEE/RSJ International Conference on Intelligent Robots and Systems*, 2014, pp. 3067–3072.

[12] H. Bayram, J. Vander Hook, and V. Isler, "Gathering bearing data for target localization," *IEEE Robotics and Automation Letters*, vol. 1, no. 1, pp. 369–374, 2016.

[13] A. Kelly, "Precision dilution in triangulation based mobile robot position estimation," in *Proceedings of the Int. Conf. on Intelligent Autonomous Systems*, Amsterdam, 2003.

[14] O. Tekdas and V. Isler, "Sensor placement for triangulation-based localization," *IEEE Trans. Autom. Sci. Eng.*, vol. 7, no. 3, pp. 681–685, 2010.

[15] D. Applegate, R. Bixby, V. Chvatal, and W. Cook, "Concorde TSP solver," *URL: http://www.math.uwaterloo.ca/tsp/concorde.html*, 2017.

[16] G. N. Frederickson, M. S. Hecht, and C. E. Kim, "Approximation algorithms for some routing problems," in *Foundations of Computer Science, 1976., 17th Annual Symposium on*. IEEE, 1976, pp. 216–227.

[17] "rtl-sdr software," http://osmocom.org/projects/sdr/wiki/rtl-sdr, 2017 (accessed June 15, 2017).

[18] H. Bayram, N. Stefas, and V. Isler, "Aerial radio-based telemetry for tracking wildlife," Department of Computer Science and Engineering, Univeristy of Minnesota, Tech. Rep. 17-004, 2017.

[19] D. Bhadauria, O. Tekdas, and V. Isler, "Robotic data mules for collecting data over sparse sensor fields," *Journal of Field Robotics*, vol. 28, no. 3, pp. 388–404, 2011.